

## Submarine Thermal Springs on the Galápagos Rift

John B. Corliss, Jack Dymond, Louis I. Gordon,  
John M. Edmond, Richard P. von Herzen, Robert D. Ballard,  
Kenneth Green, David Williams, Arnold Bainbridge,  
Kathy Crane, Tjeerd H. van Andel

The presence of active convective circulation of seawater through newly formed oceanic crust along the Galápagos Rift was proposed by Sclater and Klitgord (1). Such circulation was strongly indicated by profiles of bottom water temperatures and measurements of heat flow obtained by Williams *et al.*

benthic fish floated to the surface, were attributed to volcanic eruptions or associated hydrothermal activity (4).

The existence of thermal springs associated with volcanism at midocean spreading centers was first suggested 12 years ago (5). Early speculations about the process were based on the occur-

**Summary.** The submarine hydrothermal activity on and near the Galápagos Rift has been explored with the aid of the deep submersible *Alvin*. Analyses of water samples from hydrothermal vents reveal that hydrothermal activity provides significant or dominant sources and sinks for several components of seawater; studies of conductive and convective heat transfer suggest that two-thirds of the heat lost from new oceanic lithosphere at the Galápagos Rift in the first million years may be vented from thermal springs, predominantly along the axial ridge within the rift valley. The vent areas are populated by animal communities. They appear to utilize chemosynthesis by sulfur-oxidizing bacteria to derive their entire energy supply from reactions between the seawater and the rocks at high temperatures, rather than photosynthesis.

(2), and by deep tow observations made by Klitgord and Mudie (3) on the *Southtow* expedition in 1972. Water temperature anomalies over the spreading axis were attributed to plumes of warm water rising from hydrothermal vents. Systematic fluctuations of heat flow in sediments 5 to 30 kilometers south of the spreading axis, and linear arrays of mounds on these sediments, were interpreted as resulting from cells of hydrothermal circulation in the underlying basaltic crust. Abundant microearthquake activity and a fish kill, in which dead

fish floated to the surface, were attributed to volcanic eruptions or associated hydrothermal activity (4).

References of metalliferous deep-sea sediments (6), altered midocean ridge basalts (7), and anomalous heat flow associated with midocean ridges (8). Explicit models for submarine hydrothermal systems were based on features of the chemistry of dredged basalts with contrasting cooling histories (9), models of hydrothermal

convective cooling of the oceanic crust (10, 11), and observations of exposed oceanic crust in ophiolite complexes (12). Recently, studies have been conducted on basalt-seawater interaction (13–17), physical models of seawater hydrothermal convective systems (18, 19), and global budgets of hydrothermal heat and metals (20–22). Further studies have been made of metalliferous sediments (23–25) and hydrothermal effects in ophiolites (26–28), and searches have been made at sea for active hydrothermal systems (2, 4, 29).

On the basis of the evidence gathered on the *Southtow* cruise, we proposed a diving program on the Galápagos Rift to the International Decade of Ocean Exploration Office of the National Science Foundation. A detailed bathymetric survey conducted by the U.S. Naval Oceanographic Office with a multibeam sounding (MBS) system (30), and results of the *Pleiades* cruise in 1976 (31–37), established the area as a prime site for a comprehensive study of midocean ridge hydrothermal activity with a submersible.

In February and March of 1977, we made a series of 24 dives in the deep submersible *Alvin* on the 2.5-kilometer-deep axis of the Galápagos Rift (Fig. 1A). These dives enabled us to make direct visual observations of the area, to make small-scale physical measurements, and to obtain samples of fluids and related deposits at thermal-spring vents on the sea floor. Our goal was not only to prove the existence of hydrothermal plumes by firsthand observation, but also to explore phenomena associated with the convective circulation of seawater beneath the ocean floor. We thus attempted to (i) locate active hydrothermal vents on the sea floor and relate their distribution to the local and regional crustal tectonic fabric; (ii) determine the heat and seawater budgets of hydrothermal systems; (iii) characterize and quantify the fluxes of matter from the oceanic crust into the deep-sea environment; (iv) study the in-

J. B. Corliss, J. Dymond, and L. I. Gordon are at the School of Oceanography, Oregon State University, Corvallis 97331. J. M. Edmond is in the Department of Earth and Planetary Sciences, Massachusetts Institute of Technology, Cambridge 02139. R. P. von Herzen, R. D. Ballard, and K. Green are at the Woods Hole Oceanographic Institution, Woods Hole, Massachusetts 02543. D. Williams is at the U.S. Geological Survey, Federal Center, Denver, Colorado 80225. A. Bainbridge and K. Crane are at the Scripps Institution of Oceanography, La Jolla, California 92037 (K. Crane's present address is Woods Hole Oceanographic Institution, Woods Hole, Massachusetts 02543). Tj. H. van Andel is in the Department of Geology and Geophysics, Stanford University, Stanford, California 94305.

teraction of these fluids with seawater, and the processes of precipitation, dispersal, and sedimentation of resultant solid phases; (v) characterize the hydrothermal fluids chemically, and to relate these observations to models of the kinetics and thermodynamics of water-rock interaction; and (vi) quantify the fluxes of matter from seawater into the rocks during alteration of the crust.

In the course of our explorations, we discovered extraordinary communities of organisms living in the thermal vent areas at the rift axis and we describe some of these animals later in this article.

## Geology of the Rift Valley

During the *Alvin* diving expedition a towed camera sled (*Angus*) was used from the escort vessel RV *Knorr* to obtain about 70,000 color photographs of the bottom, along a series of closely spaced tracks (38, 39). Additional color photographs supplemented by visual observations were obtained on 11 dives of the submersible *Alvin*, in four of which we made long traverses of the terrain. The camera sled and submersible were precisely navigated within an acoustic transponder net tied into the 1976 deep tow grid. The precision of the *Alvin* and

*Angus* navigation is approximately 10 to 20 meters.

The Galápagos divergent plate boundary at 86°W lies in a small rift valley, about 3 to 4 km wide, 200 to 250 m deep, and trending east-west (Fig. 1B) (3, 32). The valley resembles the inner rift of the Mid-Atlantic Ridge at 36°N (40), except the latter is contained in a 30-km-wide rift valley, whereas the Galápagos Rift is bordered by the gently outward sloping flanks of the ridge.

The Galápagos Rift valley is bordered on the north and south by steep escarpments produced by normal faulting. The north wall is straight and continuous; the south wall is replaced west of 86°W by a deep elongate trough resulting in a wall offset about 400 m to the south. The floor of the rift valley (Fig. 1B), at a mean depth of about 2450 m, contains a single, straight, east-west trending axial ridge, rising about 20 m above the mean depth of the valley. In addition, there are several long and narrow marginal ridges, similar in height and mean width to the axial ridge. The axial ridge is essentially free of sediment and consists of the youngest volcanics in the area. Toward the north and south, both the sediment cover and the degree of visible surficial alteration of the volcanics increase.

Two principal lava types can be distinguished in the *Angus* photography: pillow and sheet flows (39). The sheet flows

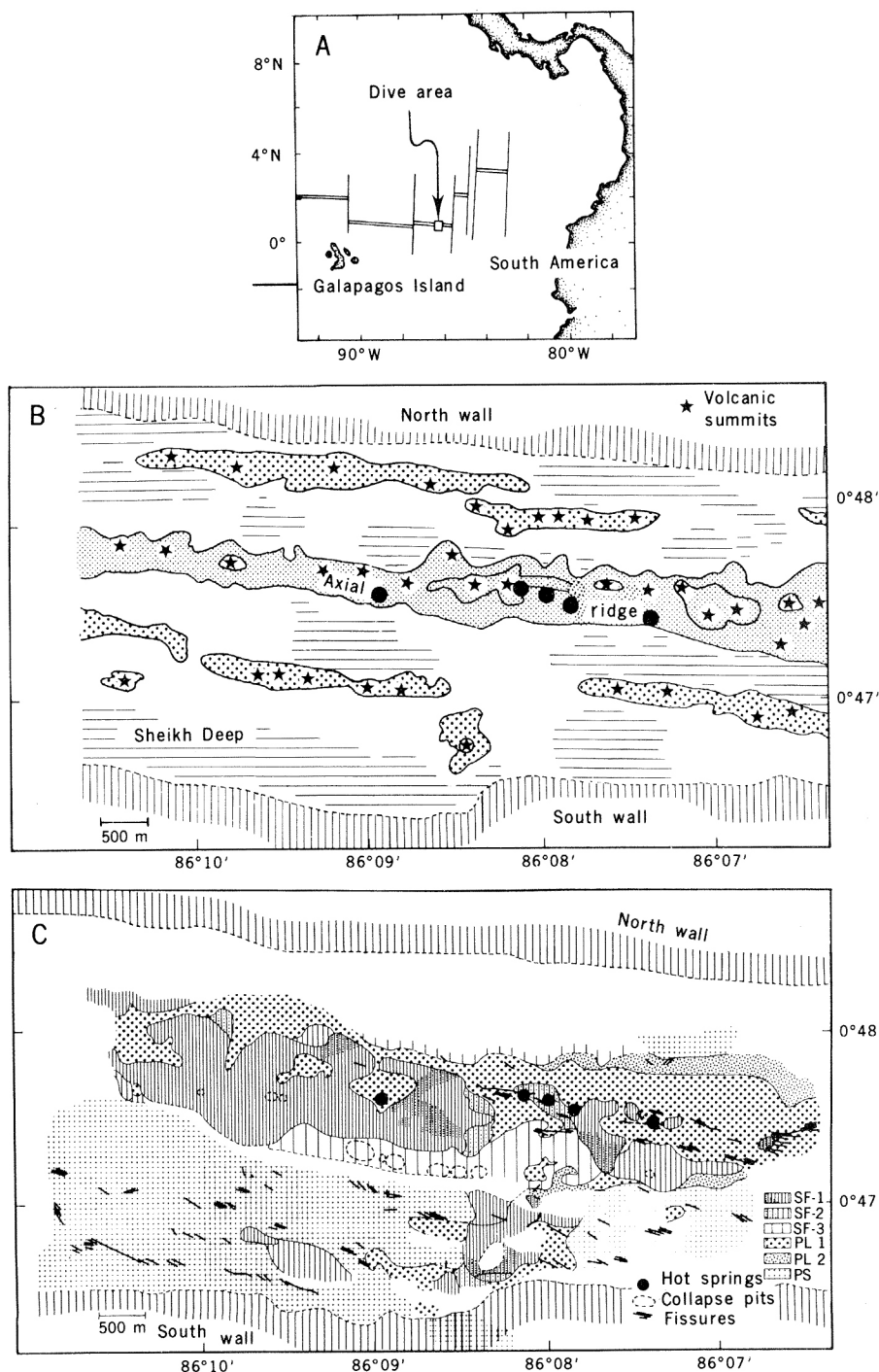


Fig. 1. (A) Location of the survey area. (B) Morphological units of the rift valley of the Galápagos Rift near 86°W, based on analysis of the multibeam bathymetric chart with 2 fathoms (3.65 m) contour interval. Axial ridge and marginal ridges are stippled, and main axial volcanoes are indicated with denser patterns. Marginal deeps are horizontally shaded, while the north and south wall are indicated with vertical bars. The depth of the axial ridge is about 2500 m. The vent areas are named, from west to east, Clambake, Clambake II, Dandelions, Oyster Bed, and Garden of Eden. (Clambake II appeared dead from *Alvin*, but a small area of living animals was found in the *Angus* photographs.) (C) Volcanic units of the rift valley of the Galápagos Rift near 86°W. Symbols: SF1, youngest volcanoes consisting mainly of fresh glassy sheet flows free of sediment with minor, fresh, pillow lavas; SF2, slightly older sheet flow unit with associated pillow lavas, free of sediment; SF3, oldest sheet flow units, with altered glass and moderate sediment dusting; PL1, pillowed flows forming the main basement of the axial ridge, older than units SF1 and SF2, and possibly approximately contemporaneous with SF3, moderately dusted with sediment; PL2, even older pillow basalts, not associated with present axial volcanism, possibly preceding sheet flows of SF3; and PS, marginal volcanic terrain (pillowed and sheet flows) < 75 percent covered with sediment. Geology is based mainly on towed camera runs and is somewhat generalized.

are generally flat and range from smooth to wrinkled andropy. The pillow terrain shows much more relief, up to 10 m or more, and generally consists of large (up to 1 m or more) pillows. Extensive, blocky lava is common in sheet flows, but also occurs occasionally in pillowed terrain, usually near the flow fronts.

We have recognized a sequence of relative ages on the basis of (i) the degree of alteration of the basalt surface, (ii) the freshness of glass, (iii) the abundance of small glassy buds on the pillows, and (iv) the amount of sediment cover. The spreading rate of the Galápagos Rift, determined from magnetic anomalies, is approximately 35 millimeters per year (*1*,

*3*), whereas the sedimentation rate in the region at the ridge depth is about 5 centimeters per 1000 years, according to measurements of sediment thickness on the crust north and south of the spreading axis.

The virtual absence of sediments on the youngest units, which are commonly not even dusted with detritus, suggests a maximum age of less than 100 years. At the inner boundary of the sediment-covered valley margins, the sediment cover is thick enough so that only the tops of the larger pillows emerge, indicating a minimum age of 10,000 years or more at a distance of 500 m or so from the axis, in reasonable accord with a

crustal age of about 14,000 years estimated from the spreading rate.

As shown in Fig. 1C, the center and western part of the axial ridge is covered with the youngest rocks; mainly sheet flows (SF 1 to SF 3) associated with a minor amount of equally fresh pillowed flows. The sheet flows surround and lap onto slightly older masses of pillowed terrain that are somewhat altered and have much less glass. The two larger hills on the axial ridge, as well as most summits, consist of this slightly older pillowed terrain that was inundated by a very recent sheet flow, perhaps 10 to 50 years ago.

The fresh sheet flows extend well

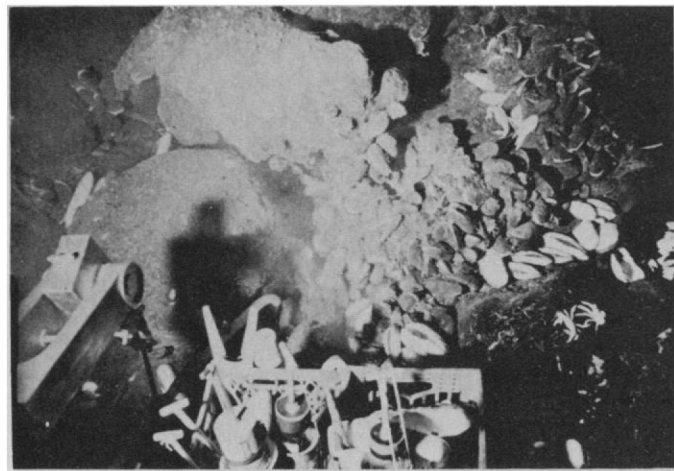


Fig. 2 (left). Clambake vent area. The water flows from the vent at  $\sim 12^{\circ}\text{C}$  mixing immediately with ambient bottom water at  $\sim 2^{\circ}\text{C}$ , precipitating in a milky white plume which served as a visual signal of nearby vents to observers in *Alvin*. The large clams and mussels dominate this vent area. The area of active venting is roughly circular, about 50 meters in diameter. The light-emitting diode display in the lower left corner provides depth, gyro heading, dive number, and time. [Photo by *Alvin*'s automated camera]

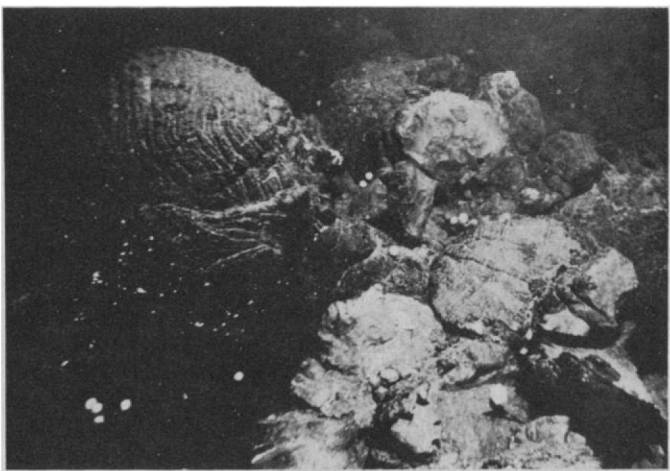


Fig. 3 (right). The Dandelions vents. The small spherical animals in the lower left corner have not been identified. Such animals were found in each vent area; at the Garden of Eden, they lived around the periphery of the vent area outside the area of venting water. They suspend themselves from the rocks above the bottom on very fine weblike "legs" not visible in this photograph. The absence here of large filter feeders common to other vent areas is very significant: because there is no hydrogen sulfide in the venting fluids here (presumably because of more extensive subsurface mixing), the sulfur-oxidizing bacteria, which are the normal primary producers supporting the filter feeders, are not present. [Photo by J. B. Corliss]

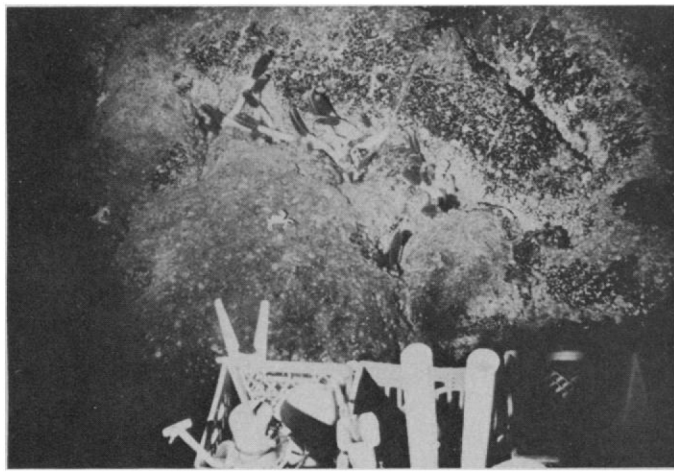


Fig. 4 (left). The Garden of Eden. This appears to be the youngest area, where water with temperatures to  $17^{\circ}\text{C}$  flows from the fissures bounding flat, lobate pillows of a very fresh-appearing lava flow. Limpets and Pogonophora are well established in these fissures. In this area *Alvin* was surrounded by the shimmering caused by mixing of the warm and cold water. [Photo by *Alvin*'s automatic camera]

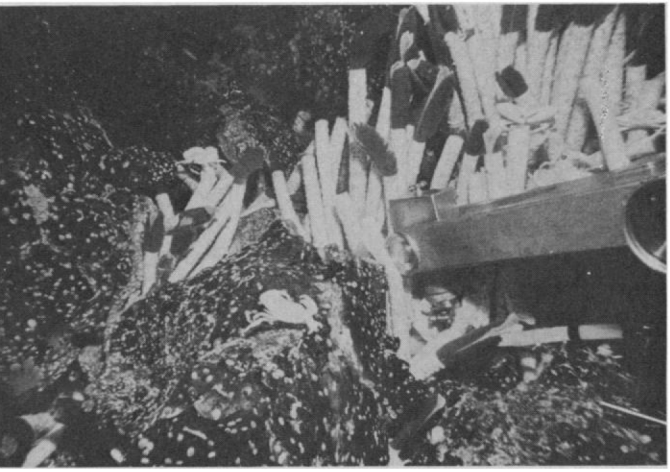


Fig. 5 (right). Oyster Bed vent area. *Alvin*'s mechanical arm inserts the water-sampling probe into a cluster of Pogonophora living in the warm water flowing from the rocks. The cancrin crab (center) was common in all vent areas; the round white animals attached to the rocks are members of a new family of limpets. Abundant mussels of the same species as those in Clambake, but smaller, are also present in this vent field. [Photo by J. Edmond]

beyond the boundaries of the axial ridge into the marginal depressions. Locally, distinctions can be made between two successive phases of the youngest sheet flows. The older sheet flow sequence south of the axial ridge is marked by numerous collapse pits, some several hundred meters in diameter, up to 20 m deep, and floored with smooth pahoehoe. The lava surface is frequently encrusted with bright yellow efflorescences and closely resembles, in morphology and flow forms, the Halmaumau lava pits on the island of Hawaii. Exposures in the walls of the deeper pits suggest a thickness of the sheet flows in excess of 25 m. Collapse pits also occur in the youngest sheet flows, but these pits are generally smaller.

Fissuring is widespread in the marginal depression and ridges and affects both pillowed and sheet flows, but it is rather uncommon on the axial ridge. The youngest flow units are not fissured at all; fissuring is common only in the slightly older eastern pillow units. The fissures in the rift valley range from hairline cracks to fissures several meters wide; occasionally they are developed as small horst-and-graben structures with vertical offsets of a few meters. It is likely that many of the individual fissure crossings in our photographs form parts of long fissure systems. Crane (32), using a side-scan sonar, described fissure systems with lengths of 500 m to a few kilometers.

### Hydrothermal Vents at the Rift Axis

The four active vent areas sampled (see Fig. 1) range in dimension from 30 to 100 m and are all located on or near the axial ridge in pillow basalt slightly older than the youngest sheet flow, near the contact with this unit. In Clambake and Dandelions, the pillows are typical bulbous forms (Figs. 2 and 3), whereas in the Garden of Eden (Fig. 4) the pillows are flat and lobate, transitional to a sheet flow. The Oyster Bed vents (Fig. 5) are located in high-relief, talus-covered terrain produced by faulting.

All vent areas are near (within 10 to 50 m) small vertical fault scarps or within grabens with offsets of a meter or so. Small fissures (2 to 10 cm wide) which cut across pillows can be traced for several meters near some vent areas. Large open fissures do not serve as vents for warm water; in numerous crossings of such features no flow of warm water was detected. In all cases, the hydrothermal fluids are streaming up from the normal openings between pillows found in a rough pillowed surface or between talus blocks in Oyster Bed.

The shimmering produced by mixing of the warm water with the cold bottom water was the most striking physical feature of the vents. In addition, a very faint milky white precipitate could be seen forming in the rising fluid less than a meter above the bottom, and the rocks were coated with a thin manganese oxide coat-

ing where the warm water was in contact with them. The maximum temperatures measured differed between vent areas, from 7°C in Dandelions to 17°C in the Garden of Eden, compared to ambient bottom water temperatures of 2.0°C.

A long-term temperature recorder with thermistor sensors was left at one of the Clambake vent sites for about 10 days. One sensor, placed in the vent at the sea floor, recorded a relatively steady and high temperature ( $10.5^{\circ} \pm 1.0^{\circ}$ C), over the entire period. Another sensor about 50 cm above the other recorded lower and more variable temperatures ranging from 4° to 6°C with excursions to 8°C, reflecting the turbulent entrainment of 2°C ambient bottom water into the warm water.

Fluid flow rates were measured at three different "vents," two in the Garden of Eden and one in Clambake. The flow rates, estimated by visual observations from *Alvin* on a vane-type flowmeter placed over these individual vents, range from 2 to 10 liters per second. The "vents" were areas within the vent fields where a sufficient flow was concentrated to allow measurement of a vertical current. Within the vent fields, warm water was flowing from essentially every natural opening in the rocks at various rates, making estimates of total discharge based on direct measurements of flow rates difficult.

This warm water rising from the vent areas formed thick layers or plumes of

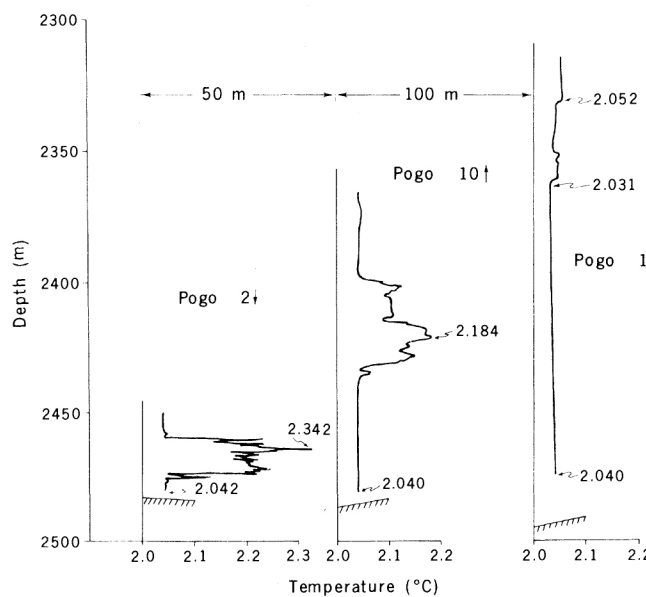
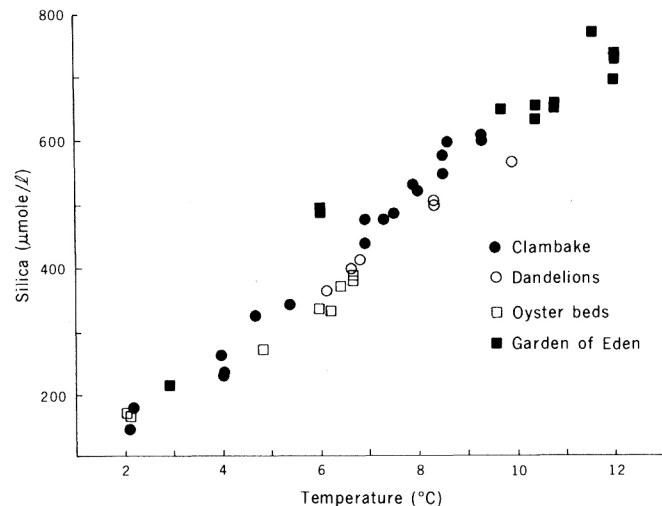


Fig. 6 (left). Clambake plume profiles. An acoustically navigated CTD (a device for measuring conductivity, temperature, and depth) was towed horizontally through the vent area and raised and lowered obliquely to provide a three-dimensional view of the plume. The departure from the vertical of each profile is given and bottom depths are marked for the start and end of each profile. Fig. 7 (right). Silica plotted against temperature: all the ridge crest data are utilized. The ambient values are 165  $\mu\text{mole per liter}$  and 2.04°C. The extension of the mixing line intersects the quartz solubility curve at  $\approx 300^{\circ}\text{C}$ . If the assumptions of the quartz geothermometer are valid, this indicates that the seawater in all vent areas last equilibrated with rocks at depth at this temperature. This "end-member" fluid rises, mixing with descending cold water which, because of its greater density and resulting pressure head, will readily flow laterally into the rising subsurface plume.



varying horizontal and vertical extent which were detected to 180 m above the bottom. These plumes were detected on the *Southtow* and *Pleiades* cruises, and on the diving expedition (*Knorr* 64) by thermistors mounted on the *Angus* camera sled. A transponder-navigated instrument (CTD) which recorded conductivity, temperature, depth, and dissolved oxygen, was towed through the vent areas to map the horizontal and vertical structure of the plumes (Fig. 6). Data of this type will be required to determine the total fluid and thermal flux of individual vent areas.

### Chemistry of the Hydrothermal Fluids

Our *Alvin* sample probe, with a thermistor attached, was inserted into the openings from which the water flowed, and the fluids were sampled by pumping the water through a variety of valves which could direct the flow through filters, if desired, and then into sample bottles. Downstream from the sampler, the water flowed past sensors for measuring temperature, conductivity, dissolved oxygen, and pH. These data were displayed and recorded continuously, along with other dive parameters, on magnetic tape within the submarine. Eighty-eight approximately 9-liter samples of hydrothermal fluids and associated ambient water were collected, and more than 2000 subsamples have been distributed for laboratory analysis on shore, to supplement the extensive shipboard analytical program.

The temperature and chemistry of the water samples can be considered the result of two mixing processes. First, the water flowing up through the rocks prior to venting through the sea floor can be considered a mixture of some initial hydrothermal fluid formed by water-rock interactions at depth, and cooler descending seawater entrained with this warm water as it rises through the rocks (subsurface mixing). Second, the water flowing from the rocks immediately begins mixing with ambient seawater, and varying amounts of this ambient water are entrained prior to sampling (surface mixing). The subsurface and surface mixing are essentially one single mixing process involving only two ultimate end-members: (i) the fluid produced at depth through interactions with the rocks and (ii) ambient seawater.

For conservative components (that is, those not added to or removed from the fluids during ascent and mixing), if the subsurface end-member has uniform properties within a single vent area or several vent areas, all samples will fall on a single mixing curve. This is clearly the case for silica in all vent areas (Fig. 7). The scatter may be due to the temperature uncertainty ( $\approx \pm 0.5^\circ\text{C}$ ) caused by differing proportions of ambient waters being entrained during the sampling interval. Hence the silica data are probably a better measure of the degree of dilution; certainly graphs in which the other elements are plotted against silica show significantly less scattering than when they are plotted against temperature.

The extrapolation of the silica-temper-

ature line intersects the quartz solubility curve for distilled water at 1000 atmospheres (41–43) at about  $300^\circ\text{C}$ ; it coincides with the curve for opal in the range 50° to  $70^\circ\text{C}$ . Although experimental seawater-basalt hydrothermal systems at temperatures below  $300^\circ\text{C}$  achieve equilibrium with amorphous silica rather than quartz (13, 16), above this temperature the quartz grows in the solution (14), and quartz is a common phase in hydrothermally altered oceanic crustal rocks (44, 45). It is possible that there is a secondary reaction with the glassy basalts in the upper part of the section. In addition, this extrapolation does not reflect departures from linearity of the enthalpy of seawater above  $200^\circ\text{C}$ , or uncertainties in the solubility of silica in seawater at these temperatures. Resolution of these effects may be possible by comparison with other chemical and isotopic measures of solution temperatures.

Other elements have a variety of relationships with temperature and silica. The amount of barium increases strongly in all the vent fields (Fig. 8); however, the Ba/Si gradient in the Clambake area is more than twice that determined for the other three vent fields. The concentration of manganese (46) is strongly correlated with barium, with values as high as 31 micromoles per liter. For lithium, by contrast, the Clambake, Garden of Eden, and Dandelions waters fall on one line with Oyster Beds having a lower Li/Si gradient. The values range to more than twice ambient. These variations among vent fields reveal differences in subsurface high-temperature fluid com-

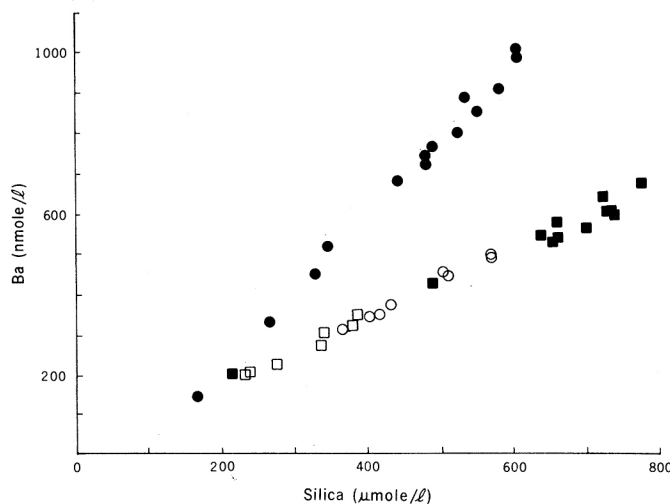
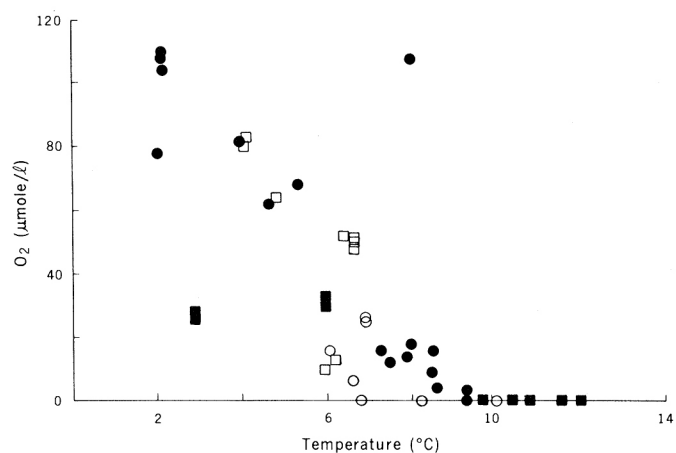


Fig. 8 (left). Barium plotted against silica. The two distinctive mixing curves indicate that the Clambake vent area has a different "end-member" fluid composition from the other vent areas. Clambake is  $\approx 1600$  m from Dandelions, the nearest of the three, which are separated from each other by less than 700 m. Manganese has the same relationship as barium with silica. Such springs are the major source of manganese in the oceans and are an important source of barium.

Fig. 9 (right). Oxygen concentration plotted against temperature. The shipboard oxygen data suggest that the water is anoxic as it flows from the rocks, and that the oxygen present in our samples results from surface mixing with ambient oxygenated bottom water. Reaction with hydrogen sulfide during the interval between sampling and analysis may affect this relationship, but preliminary data in situ from the CTD-O<sub>2</sub> system on *Alvin* suggest that this effect is small.



positions that must be related to variations in physical and chemical conditions of the water-rock interactions.

The amount of calcium increases more than 1 percent, the Clambake area again having a higher concentration than the rest. Strontium is constant over all the vents to within the measurement precision (0.25 percent). Magnesium shows a uniform decrease by about 3 percent over the range sampled, in agreement with predictions that magnesium is removed from seawater during hydrothermal circulation in rock-dominated systems (13). The magnesium-temperature line extrapolates to a "zero magnesium" temperature of about  $280^\circ \pm 20^\circ\text{C}$  in agreement with the quartz geothermometer value. Though neither is conclusive, the coincidence of these temperatures tends to support their individual validity, suggesting that the seawater last equilibrated with the rocks at a temperature of about  $300^\circ\text{C}$ .

Hydrogen sulfide also shows distinctive distributions in each vent field. None was detected in Dandelions. The Clambake values range up to  $20 \mu\text{mole}$  per liter, Garden of Eden to  $60 \mu\text{mole}$  per liter, and Oyster Beds to  $160 \mu\text{mole}$  per liter. The concentrations of elements which form extremely insoluble sulfides under these conditions are concomitantly low. Data for iron give a range of values equivalent to iron to manganese ratios of from three to several hundred. It appears that nickel, copper, and cadmium are completely depleted in the subsurface fluids and are added only by surface mixing with ambient water. Abundance patterns for the rare earth elements show a strong positive europium anomaly which may reflect reduction of  $\text{Eu}^{3+}$  to  $\text{Eu}^{2+}$  and preferential extraction from the rocks under these reducing conditions.

The effects of surface mixing of ambient water and vent water are clearly shown in Fig. 9. Dissolved oxygen from the ambient bottom water often coexists in the samples with hydrogen sulfide in disequilibrium. The trend toward zero oxygen at  $8^\circ$  to  $10^\circ\text{C}$  indicates either that the vent water contains essentially no oxygen prior to emerging from the rocks, or that extensive reaction between oxygen and hydrogen sulfide occurs in the samples subsequent to collection. The data from the oxygen probe in the sampling system on *Alvin* minimize the latter possibility since the difference between these data and the shipboard measurements on identical samples is less than  $25 \mu\text{mole}$  per liter. Nitrate, another oxidized species found in disequilibrium with sulfide in the samples, is linearly

correlated with oxygen, extrapolating to zero at approximately minus  $25 \mu\text{mole}$  of oxygen per liter, and is presumably supplied by surface mixing with ambient water. Scanning-electron-microscope analysis of material filtered from the vent fluids shows the milky precipitate appearing in the vent fluids to be elemental sulfur, presumably forming by oxidation of hydrogen sulfide.

The acidity of subsurface fluids is reflected in the alkalinity changes during surface mixing. As the solutions mix with ambient water and cool, the alkalinity decreases by 25 microequivalents per liter per degree Celsius. The total  $\text{CO}_2$  increases by  $25 \mu\text{mole}$  per liter per degree Celsius, indicating a significant flux of  $\text{CO}_2$  from the mantle. Isotopic measurements should allow us to quantify the flux more precisely.

The extent of entrainment of descending ambient seawater appears to vary between vent fields, being greatest in Dandelions and probably least in Garden of Eden. The degree of subsurface mixing exerts a profound effect on the redox systems in general and on elements such as iron, copper, nickel, zinc, and cadmium in particular. Transport of these elements in solution in the presence of large amounts of sulfide (in the millimolar range at  $300^\circ\text{C}$ ) requires acidic, high-temperature conditions (47). If, indeed, the iron to manganese ratio of 3:1 in metal-rich sediments of the ridge is representative of the average exit value of hydrothermal systems (6, 23-25) then hot springs at greater than  $100^\circ\text{C}$  may be common, perhaps as short-lived phenomena following volcanic eruptions, involving interaction of seawater and flow interiors and dikes as proposed (9). These observations have implications for the formation of massive sulfide deposits by submarine hydrothermal systems.

The extent of inferred subsurface mixing and cooling is more than sufficient to preclude transport of sulfide-forming elements to the sea floor, but is not (except for the case of Dandelions) enough to produce an oxidizing system. In systems such as the Dandelions, since the solutions will be oxidizing and, because of lack of relative buoyancy, quite slow-moving, conditions around the exits should provide the ideal regime for formation of the very pure manganese oxide crusts discovered on the Mid-Atlantic Ridge (48) and elsewhere on the Galápagos spreading axis (49). Since the manganese is maintained in reduced form in the vent regions sampled and the ascent rates are very rapid, no such crusts were observed.

The helium isotopes have proved use-

ful for understanding the global implications of our observations of these thermal springs. Jenkins *et al.* (50) showed that helium exhibits a regular increase proportional to silica and temperature. Combined with the best estimate for the total flux of helium-3 through the oceans to the atmosphere of Craig *et al.* (51), and assuming that this flux is all produced from hydrothermal systems at the spreading center with similar relations between helium and heat, we can estimate global hydrothermal flux of heat (50). This gives a flux of about  $5 \times 10^{19}$  calories per year, in close agreement with recent estimates based on heat flow (20, 22, 52).

The flux of the elements into or out of the ocean has been computed and compared to the river input. Using the same reasoning as for heat flux, we can use the flux of  $^3\text{He}$  to calculate these values for elements we have measured. Of course, it is by no means clear that the existing data are representative of all ridge crest hydrothermal systems. However, the results are impressive (Table 1). The ridge crest hydrothermal system is the major sink for magnesium and the major source for sedimentary manganese and for lithium. It provides a substantial proportion of the silica and barium. It is a minor source of calcium and  $\text{CO}_2$  and a significant sink for alkalinity. The systems we measured are also sinks for copper, nickel, and cadmium, but the dependence of the redox behavior of the systems on their physical characteristics—that is, flow rates and exit temperatures—makes it difficult to generalize from our data.

The heat to mass ratios for conservative elements also provide insight into the extent of interaction of seawater with the crust. Combined with data for the concentration of these elements in the magma and the heat content of the magma, they provide strong constraints on the depth of water penetration and the extraction of heat, gases, and other rock components (53).

#### Biological Observations in the Vent Areas

Large white objects identified as clamshells appeared in a few of the *Pleiades* deep tow photographs taken along the axial ridge (54). Observations from *Alvin* showed these to be evidence of highly productive communities of exceptionally large and densely spaced animals living within the hydrothermal vent areas. These animals provided a valuable indicator of thermal vents in our *Angus* photographs. We collected some of the animals amenable to sampling with the

equipment available, primarily large clams and mussels, limpets, and tube worms, and also collected water samples and filtered suspended matter for biological studies (55).

The clams resemble an unusual family, the Vesicomyidae, which is probably allied to the common successful shallow-water veneroid clams such as quahogs. Vesicomyids have a considerable zoogeographic and bathymetric range (that is, greater than 3000 m), and their length may be only a couple of millimeters or up to 150 mm. They were found only in one active vent area, where they are of somewhat uniform large size, from about 150 to 300 mm, and cover large patches of the ocean floor filling the depressions between basalt pillows.

The mussels all appear to belong to the same new genus and species of the family Mytilidae. Their anatomy is distinctly different from shallow-water forms and from other known deepwater forms. The mussels were abundant in the Clambake where they averaged from 100 to 150 mm in length, and in the Oyster Bed where they ranged from 7 to 53 mm in length.

The limpets belong to a new gastropod family; they resemble members of the Calyptraeidae, a group in which abyssal species are unknown. However, there are some unusual anatomical features that indicate an affinity with more primitive groups of mollusks. In the new species, the gills are large and evidently used for filter feeding by ciliary currents, as in the Calyptraeidae. They are commonly attached to rock surfaces not occupied by the mussels in Oyster Bed and are abundant in the Garden of Eden where they line the interpillow fissures from which the warm water flows.

The tube worms belong to the class Vestimentifera of the phylum Pogonophora. The phylum is mostly restricted to the ocean depths. The Vestimentifera are the largest of the Pogonophora and two species of a single genus have been described. The hot-spring specimens (Figs. 4 and 5) represent a new genus of Vestimentifera and are the largest members of the class and phylum, with chitinous tubes ranging up to 338 mm in length and 25 mm in diameter. They possess a plume of fused tentacles that can be extended from the tube, presumably for respiration. They lack a gut or other visible digestive system, a characteristic of the Pogonophora, and live attached to rocks directly in the flow of warm waters from the vents.

In each vent area, we observed and photographed what appeared to be an apparently undescribed species of ophid-

Table 1. Hydrothermal flux of various components to the oceans. The global hydrothermal flux for each element is estimated by multiplying the mass to heat ratio in the fluids for the element by the estimated global hydrothermal heat flux. The hydrothermal flux of  $^3\text{He}$  is assumed equal to the total oceanic flux of  $^3\text{He}$ , and is used to estimate the global hydrothermal heat flux. Values for the global river flux (or global sedimentation rate) are given for each component for comparison ( $A_t$  = alkalinity). References are given in parentheses.

Element	Mass to heat ratio (mole/cal)	Hydrothermal flux (mole/year)	Global river flux (mole/year)	Global sedimentation rate (mole/year)
$^3\text{He}$	$22 \times 10^{-18}$	$1.08 \times 10^3$ (48)		
Li	$2.6 \times 10^{-9}$	$130 \times 10^9$	$13.5 \times 10^9$ (63)	
	$1.5 \times 10^{-9}$	$75 \times 10^9$		
Mg	$-190 \times 10^{-9}$	$-9.3 \times 10^{12}$	$5.4 \times 10^{12}$ (64)	
				$12 \times 10^{12}$ (64)
Ca	$-85 \times 10^{-9}$	$4.2 \times 10^{12}$		
	$48 \times 10^{-9}$	$2.4 \times 10^{12}$		
Ba	$130 \times 10^{-12}$	$6.4 \times 10^9$	$1.4 \times 10^{10}$ (65)	
	$49 \times 10^{-12}$	$2.4 \times 10^9$		
Si	$57 \times 10^{-9}$	$2.9 \times 10^{12}$	$7.1 \times 10^{12}$ (64)	
$A_t$	$-25 \times 10^{-9}$	$-1.3 \times 10^{12}$		$30 \times 10^{12}$ (64)
$\text{CO}_2$	$25 \times 10^{-9}$	$1.3 \times 10^{12}$		
Ni	$-0.5 \times 10^{-12}$	$-25 \times 10^{-6}$		
Mn	$3.9 \times 10^{-9}$	$190 \times 10^9$	$2.4 \times 10^9$ (66)	
	$1.5 \times 10^{-9}$	$74 \times 10^9$		$52 \times 10^9$ (67)

iod fish swimming in the rising plumes of warm water. This fish was not observed outside the vent areas, and other fish seen outside the vents were not observed inside the active vent fields. Three benthic fish recovered on *Southtow* (4) from more than 80 dead benthic fish observed floating on the surface did not include an ophidoid, but did include species similar to those we photographed outside the vent areas.

There are many questions to be answered about these animal communities. One concerns how they locate and colonize new vents. It is clear that an individual vent area has a finite lifetime. We discovered several dead vent areas along the axial ridge, recognizable by the abundant dead clamshells that were slowly dissolving away, and by the dark manganese staining around the base of the pillow basalts. Radiometric dating of the shells suggests that the shells are no more than 10 to 20 years old (56), indicating a minimum age for the thermal springs of the same order.

The animal population at each vent area is distinctly different from the populations at other vent areas. Clams and large mussels dominate Clambake (Fig. 2); small mussels and Pogonophora are the most abundant species at Oyster Bed (Fig. 5); Pogonophora and limpets are abundant at the Garden of Eden (Fig. 4). The only abundant attached animal at Dandelions has not been identified (see Fig. 3). In addition, there were a few small mussels at the Garden of Eden, and a few decayed-appearing Pogonophora tubes in Clambake. The fact that the

mussels are all large in the Clambake and small in the Oyster Bed suggests a single separate colonization in each vent area. The differences between vents suggest perhaps a progression of successive populations culminating in the mussel- and clam-dominated communities such as Clambake I.

Perhaps the most important question about these animal communities concerns their source of food. Particular features of the Galápagos hot-spring environment, such as the depth and the abundance and size of the animals, suggest that the supportive organic nutrients could not be substantially derived from primary productivity in the surface water. Moreover, because of the high concentrations of hydrogen sulfide in these waters, a significant proportion of the organic carbon utilized within these hot-spring regions could be produced by chemolithotrophic sulfur-oxidizing bacteria.

High concentrations of sulfur-oxidizing and heterotrophic bacteria (from  $10^8$  to  $10^9$  bacteria per milliliter) were observed by epifluorescence microscopy in glutaraldehyde-preserved samples of water collected as it flowed from the vents at two hot springs (57). If one assumes that the average bacterium weighs  $10^{-12}$  gram, the concentration of bacteria in the vent waters could be 0.1 to 1 gram per liter. This flux of bacteria from the vents must be supported by the productivity of a large population of bacteria living within the rock mass, lining the walls of fissures through which the hydrogen sulfide-laden fluids ascend. They

presumably become incorporated into the fluids which ultimately flow from the rocks and past the filter-feeding mussels, clams, limpets, and Pogonophora which surround and fill the vents.

The generation time for these populations of sulfur-oxidizing bacteria in situ is not known, but, unlike phytoplankton blooms, their productivity is, presumably, continuous. Experiments with isolated cultures of these chemolithotrophs showed that they have generation times of approximately 100 hours

when grown at 15°C on sodium thiosulfate. Our data do not prove that the hot-spring animals feed on bacteria. Many sulfur bacteria similar to the species isolated from water were isolated from the Pogonophora and from the guts of mussels. Very few heterotrophs were isolated, suggesting that the feeding habits of these thermal-spring animals are somewhat different from their counterparts in areas not affected by warm water, which contain in their guts high numbers of heterotrophs, particularly species

that degrade refractory organic material.

The High concentration of bacteria in water flowing from the vents suggests that they live to some depth in the rock mass, lining fractures and fissures, and that they may significantly influence the chemistry of the system. In systems in which there is extensive subsurface mixing of ambient water, the development of an abundant surface fauna is prevented, as in Dandelions, both by oxidation of all the sulfide and by dilution and destruction of the sulfide-oxidizing bacteria, presumably inhabiting the reducing zone at depth. This, coupled with the much smaller temperature anomaly, will make such vent fields very difficult to find.

### Conductive Heat-Flow Patterns

The hydrothermal vents we have described are located at the rift axis, associated with newly erupted volcanic rocks. South of the spreading axis, we studied manifestations of hydrothermal circulation in older oceanic crust. These include a striking pattern of variations in conductive heat flow through the sediments, with maximum values associated with a band of spectacular mounds of hydrothermally deposited minerals precipitated from fluids percolating upward from the basaltic crust (Fig. 10).

More than 400 measurements of conductive heat flow have been made over this survey area on three different cruises (Fig. 10) (*Southtow*, *Pleiades*, *Knorr-64*). Because of the relatively high sedimentation rate (50 m per million years) and subdued topography, measurements were possible to within a few kilometers of the axis. The contoured heat-flow pattern is obviously two-dimensional, subparallel to the axis and topographic lineations. The break in two-dimensionality of the heat-flow pattern near the center of the map corresponds with a shift in the north-south ridge valley pattern of topography. In detail, higher values of heat flow are located over relative topographic ridges, and vice versa. A few measurements along a profile north of the ridge axis and along a line extending about 15 km south of the areal survey indicate that the oscillating patterns of heat flow extend to these regions also.

The oscillating pattern is clearly at variance with that of a simple conductively cooling plate, which would produce a monotonic decrease of heat flow with age. The observations support a mechanism of convective heat loss by hydrothermal circulation, most intense at the ridge axis.

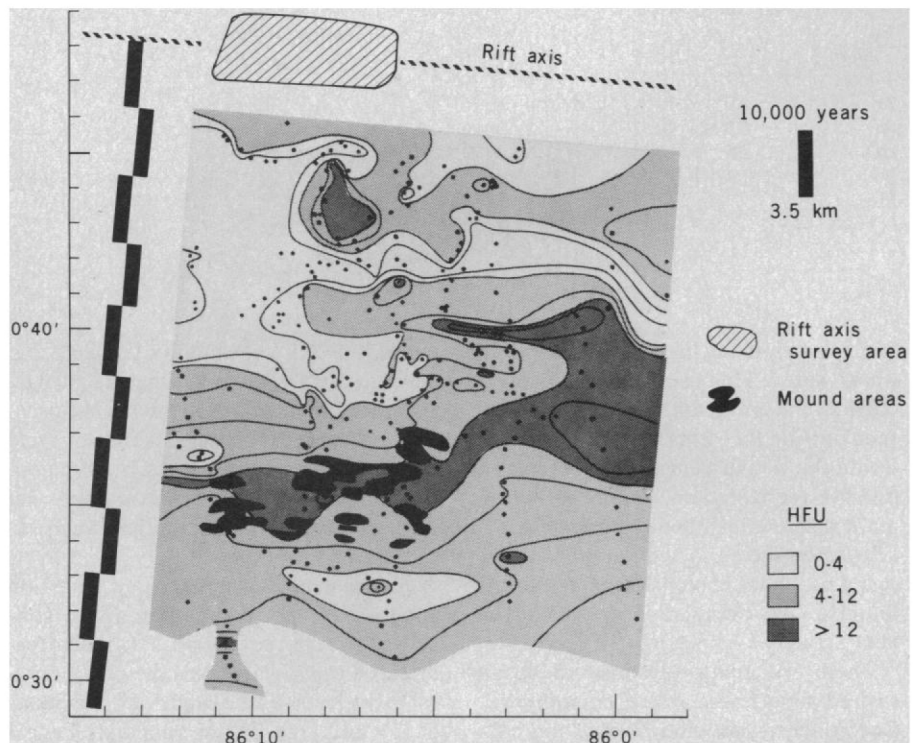
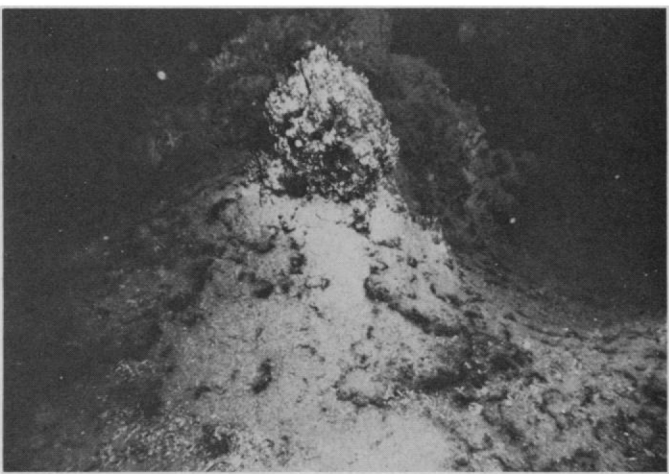


Fig. 10. A plot summarizing the heat-flow stations within the detailed survey area. The data are contoured at 2, 4, 8, and 12 HFU. The ridge crest vents are indicated along the spreading axis. The area of hydrothermal mounds is indicated on crust about 750,000 years old. These mounds are identified primarily on the basis of side-scan sonar records from the deep tow fish within the available coverage.

Fig. 11. A pinnacle on top of a 20-m-high mound. The scalloped pattern of outcropping manganese crust is typical of the undisturbed surfaces of the mounds. The interiors of such pinnacles were warm (to 6°C) and very soft, containing water-saturated nontronite and iron oxides covered by a more rigid manganese crust. Small "spikes" of iron oxides extended from the surface. These pinnacles appear to grow by deposition from the fluids flowing from the mound interiors. [Photo by D. Williams]



The variation of surface heat flow ( $q$ ) with age of the crust ( $t$ ), based on a simple model of a one-dimensional conductively cooling plate, is given as  $q = A/t^{\frac{1}{4}}$ , where  $A$  is an empirically determined constant with a value of about 12 heat flow units (million year) $^{\frac{1}{4}}$ , where 1 HFU equals  $10^{-6}$  cal per second per square centimeter (58, 59). The mean of the measured heat loss over the survey region (Fig. 10) is about 8 HFU, whereas the model predicts a mean heat loss of 24 HFU over this age range (0 to 1 million years), indicating a missing heat flux of 16 HFU on each side of the axis which could be accounted for by hydrothermal convection. Near the ridge axis, realistic geometries of the newly intruded material may modify some of the heat-loss calculations based on one-dimensional models, but not to the extent of removing such a major discrepancy.

If we consider both flanks of the ridge, this missing heat flux to 1 million years of age is equivalent to about 110 calories per second for each centimeter of ridge axis. Extrapolating this rate to the total global ridge system ( $55 \times 10^3$  km length) and correcting for the mean spreading rate, 2.7 cm/year, gives us about  $1.5 \times 10^{19}$  cal/year for the global heat loss by hydrothermal circulation. This is somewhat less than that calculated by Wolery and Sleep (20) ( $4 \pm 0.4 \times 10^{19}$  cal/year) and from the estimate based on  ${}^3\text{He}$  flux and the relation between helium and heat ( $5 \times 10^{19}$  cal/year). This difference could result from the relatively rapid sealing of the Galápagos Rift by sediment, which would inhibit convective circulation (60), but the uncertainty in the calculations is such that such sealing of the crust is not required.

#### Hydrothermal Mound Deposits

Numerous rows of hydrothermally deposited mounds, subparallel to the spreading axis, are located within the band of high heat flow from 18 to 25 km south of the rift axis (Fig. 10) in crust from 500,000 to 700,000 years old. Although produced by the same basic process, convective flow of seawater through oceanic crustal rocks, the surface manifestation of the process in this sediment-covered area is distinctly different from that of rift axis systems. Results of deep tow studies of the mounds have been presented by Klitgord and Mudie (3), Williams *et al.* (2), and Lonsdale (33), and the chemistry of the mounds, based on samples dredged on *Pleiades*, leg 2, has been discussed by Corliss *et al.* (37).

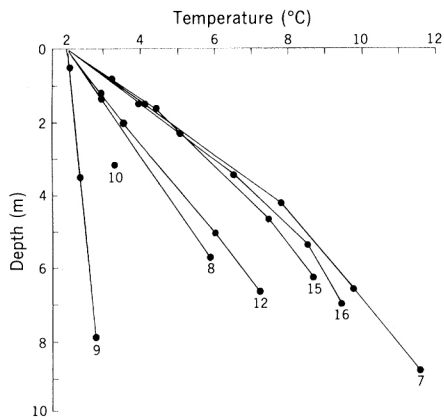


Fig. 12. Temperature gradients from piston-core measurements. All gradients have been adjusted for depth to make the bottom water temperature (2.04° to 2.06°C) consistent with extrapolation of upper gradients, except at 10 where only one temperature was successfully measured. Cores 7, 8, 15, and 16 contain mound deposits; 7, 15, and 16 show decreasing gradients with depth resulting from upward flow of interstitial water. Piston-core 9 was taken in the low-heat flow area north of the mounds (Fig. 10).

The mounds visited by *Alvin* varied in height from less than a meter to over 20 m. The small mounds typically had gentle slopes ( $< 30^\circ$ ) and were smooth or had a few small outcrops of hard ferromanganese material near their tops (Fig. 11). Away from outcrops these mounds were sediment-covered except for dark scalloped lines a few centimeters across which were found to be thin and friable ferromanganese crusts covered by a light coating of sediment. Larger mounds had correspondingly steeper slopes, sometimes vertical, with outcrops of ferromanganese material that varied from small pinnacles (Fig. 11) to cliffs a meter or two high to vertical spires and pinnacles 5 m high and 1 to 3 m across. Most mounds were roughly circular, although some mounds appeared to form essentially continuous ridges 100 to 200 m long. Generally, neighboring mounds in one row were quite similar, but an adjacent row could be quite different in size and morphology.

The geologic samples collected by *Alvin* from the mounds contain the same three hydrothermal phases found in the *Pleiades* dredge samples (37): black iron-free manganese crusts composed of mixtures of todorokite and birnessite, red-orange iron oxides containing manganese and silicon, and an aluminum-poor iron-nontronite that is normally green under reducing conditions within the mounds but can be oxidized to bright yellow when exposed to oxygenated bottom water. Iron and manganese are strongly fractionated into the non-

tronite and manganese oxides, respectively.

A common depth sequence of deposits, noted both visually and in cores and crust samples, is black manganese oxides overlying orange iron oxides which in turn overlie the green nontronite. The iron oxides often do not appear, and the exposed nontronite can be oxidized to a bright yellow. The manganese oxides appear to form a thin shell over the entire mound, often covered by a thin layer of sediment to form the scalloped outcrop pattern (Fig. 11). Drilling in the mounds area by the *Glomar Challenger* on leg 54 subsequent to our dives (61), has revealed thick beds of nontronite within and underlying the mounds, with manganese oxides nearer the surface.

In the mounds area extremely high temperature gradients, up to the equivalent of 30 HFU, were measured from the surface during *Southtow* and *Pleiades* with the heat-flow probe, and during the diving cruise on *Knorr* (*Knorr*-64) with thermistors on piston-core barrels (Fig. 12). Most of the piston-coring stations were targeted on mounds previously visited on *Alvin* dives. The descriptions of material recovered indicate that cores 7, 8, 15, and 16 sampled mound deposits, whereas cores 9 and 12 contain "normal" sediment.

All the highest thermal gradients from mounds appear to decrease significantly with depth, which suggests either non-conductive or nonsteady-state heat flux. One-dimensional modeling (62) of these gradients, assuming upward flow of pore waters gives velocities of the order of  $10^{-6}$  cm per second. Such a velocity would be difficult to detect at the sediment and water interface. Temperatures of the source water at the base of the sediment layer are calculated to be about 12° to 20°C, which is consistent with temperatures deduced from extrapolation of the conductive gradients measured in the vicinity of the mounds to the sediment and basalt interface. Measurements with a short (0.5 m) thermal probe from *Alvin* on and near the mounds also showed wide variability in temperature gradients. The highest gradients or temperatures measured, at the crests of mounds, gave calculated conductive heat flows in the range 100 to 200 HFU or higher.

The *Southtow* and *Pleiades* cruises failed to locate any temperature anomalies in the water column above the mounds and no flowing hydrothermal vents were detected by *Alvin*. However, during four dives to the mounds, a visible flow of water with temperatures be-

tween 4° and 10°C was initiated by punching holes through the crusts on the mound surfaces. In addition, the manganese concentration in bottom water and water column samples collected over the mounds on *Pleiades*, leg 2, shows a strong systematic increase in total dissolvable manganese approaching the bottom, with highest values found just a few meters above the bottom (36, 37).

Because of the low flow rates, the water collected with our sampling system from the holes was strongly diluted by ambient bottom water. The temperature anomaly of the sampled water was less than 0.5°C. Despite the strong dilution by normal bottom water, these mound waters display very strong anomalies in their radon-222 contents. Total radon-222 values as high as 388,000 disintegrations per minute per 100 kilograms were measured. The values undoubtedly reflect the interaction of the thermal waters with the relatively uranium-rich sediments of the area. Other anomalies apparent in the shipboard data are limited to subtle increases in silicon in the mounds thermal water compared to the normal bottom water.

The high internal temperatures, the presence of hydrothermal minerals, and the discovery that warm waters will emanate from holes placed in the mounds all indicate that these mounds are deposited by circulating warm water. The fact that they form in linear rows strongly suggests that faults control the location of individual mounds (33). Their relation to the regional heat-flow pattern (Fig. 10) implies that they are located over the ascending limb of a large convective cell within the oceanic crust.

## Conclusions

Venting of heated seawater was found in four vent areas along the axial ridge within the central rift of the Galápagos spreading center. The hydrothermal fluids flow from the rocks at maximum temperatures from 10° to 17°C, with measured flow rates of 2 to 10 cm/sec, and form large plumes that drift horizontally in the bottom currents. These were detected up to 150 m above the bottom where the temperature anomaly had dropped to 0.01°C.

Chemical data suggest that the interactions between the water and rocks may occur at temperatures of at least 300°C. Global hydrothermal fluxes of heat, and major and trace chemical constituents of seawater can be estimated by normalization to the  $^3\text{He}$  flux. The chem-

ical data indicate that submarine hydrothermal activity provides a major source of manganese and lithium; a minor source of calcium, barium, silicon, and carbon dioxide; and a significant sink for magnesium and alkalinity in the oceans. Nickel, copper, and cadmium are absent in the emerging vent waters because of the presence of hydrogen sulfide, which leads to the precipitation of these metals along with iron as sulfides within the rocks.

Convection of seawater in older sedimented crust south of the rift axis produces a distinctive pattern of heat flow and extensive hydrothermally deposited mounds. The mounds are formed by warm fluids percolating up from a convective cell in the underlying crust along fractures in the basalt, precipitating iron and silica in the reducing mound interiors, manganese at the bottom water interface, and carrying a significant flux of at least manganese into the bottom waters. The total hydrothermal heat loss is estimated from the heat-flow data to be 110 calories per centimeter per second, equivalent to  $1.5 \times 10^9$  cal/year globally, somewhat less than estimates based on global heat-flow patterns ( $\approx 4 \times 10^{19}$  cal/year) and on normalization to  $^3\text{He}$  flux in the rift axis vents ( $5 \times 10^{19}$  cal/year).

The exploration of the vents revealed the existence of animal communities that appear to be totally dependent on energy derived from seawater-rock reactions and chemosynthesis by bacteria for their primary productivity. These fragile communities provide a unique opportunity for a wide range of zoological, bacteriological, ecological, and biochemical studies.

## References and Notes

- J. G. Sclater and K. D. Klitgord, *J. Geophys. Res.* **78**, 6951 (1973).
- D. L. Williams, R. P. von Herzen, J. G. Sclater, R. N. Anderson, *Geophys. J. R. Astron. Soc.* **38**, 587 (1974).
- K. D. Klitgord and J. D. Mudie, *ibid.*, p. 563.
- K. C. MacDonald and J. D. Mudie, *ibid.* **36**, 245 (1974).
- J. W. Elder, *Am. Geophys. Union Monogr.* **8**, 211 (1965).
- K. Bostrom and M. N. A. Peterson, *Econ. Geol.* **61**, 1258 (1966).
- K. S. Deffeyes, in *Megatectonics of Continents and Oceans*, H. Johnson, Ed. (Rutgers Univ. Press, New Brunswick, N.J., 1970).
- M. Talwani, C. C. Windish, M. G. Langseth, *J. Geophys. Res.* **76**, 473 (1971).
- J. B. Corliss, *ibid.*, p. 8128.
- C. R. B. Lister, *Geophys. J. R. Astron. Soc.* **26**, 515 (1972).
- \_\_\_\_\_, *ibid.* **39**, 465 (1974).
- E. T. C. Spooner and W. S. Fyfe, *Contrib. Mineral. Petrol.* **42**, 287 (1974).
- J. L. Bischoff and F. W. Dickson, *Earth Planet. Sci. Lett.* **25**, 385 (1975).
- M. J. Mottl, thesis, Harvard University (1976).
- A. Hajash, *Contrib. Mineral. Petrol.* **53**, 205 (1975).
- W. E. Seyfried and J. L. Bischoff, *Earth Planet. Sci. Lett.* **34**, 71 (1977).
- W. E. Seyfried and M. J. Mottl, in *Proceedings of the Second International Symposium on Water-Rock Interaction*, H. Paquet and Y. Tardy, Eds. (Université Louis Pasteur, Strasbourg, France, 1977), vol 4, pp. 173–180.
- R. P. Lowell, *Geophys. J. R. Astron. Soc.* **40**, 351 (1975).
- C. R. B. Lister, *Tectonophysics* **37**, 203 (1977).
- T. J. Wolery and N. H. Sleep, *J. Geol.* **84**, 249 (1976).
- M. Lyle, *Geology* **4**, 733 (1975).
- D. L. Williams and R. P. von Herzen, *ibid.* **2**, 327 (1974).
- J. Dymond, J. B. Corliss, G. R. Heath, C. W. Field, E. J. Dasch, E. M. Veeh, *Geol. Soc. Am. Bull.* **84**, 3355 (1973).
- M. Bender, W. Broecker, V. Gornitz, V. Middel, R. Kay, S. S. Sun, P. Biscaye, *Earth Planet. Sci. Lett.* **12**, 425 (1971).
- G. R. Heath and J. Dymond, *Geol. Soc. Am. Bull.* **88**, 723 (1975).
- J. B. Corliss, J. L. Graf, Jr., B. J. Skinner, R. W. Hutchinson, *Geol. Soc. Am. (Abstracts with Programs)* **4**, 476 (1972).
- A. H. F. Robertson and J. D. Hudson, *Earth Planet. Sci. Lett.* **18**, 93 (1973).
- E. T. C. Spooner and C. J. Bray, *Nature (London)* **266**, 808 (1977).
- R. B. Scott, P. A. Rona, B. A. McGregor, M. R. Scott, *ibid.* **251**, 301 (1974).
- M. F. Glenn, *Int. Hydrogr. Rev.* **47**, 35 (1970).
- Cruise of the R/V *Melville*, June to July (1976).
- K. Crane, *J. Geol.* **86**, 715 (1979).
- P. Lonsdale, *Earth Planet. Sci. Lett.* **36**, 92 (1977).
- J. E. Lipton, R. F. Weiss, H. Craig, *Nature (London)* **267**, 603 (1977).
- R. F. Weiss, P. F. Lonsdale, J. E. Lipton, A. E. Bainbridge, H. Craig, *ibid.*, p. 600.
- G. Klinkhammer, M. Bender, R. Weiss, *ibid.* **269**, 319 (1977).
- J. B. Corliss, J. Dymond, M. Lyle, K. Crane, *Earth Planet. Sci. Lett.* **40**, 12 (1978).
- Tj. H. van Andel and R. D. Ballard, *J. Geophys. Res.*, in press.
- R. D. Ballard, R. H. Holcomb, Tj. H. van Andel, *ibid.*, in press.
- R. D. Ballard and Tj. H. van Andel, *Geol. Soc. Am. Bull.* **88**, 507 (1977).
- G. W. Morey, R. O. Fournier, J. J. Rowe, *Geochim. Cosmochim. Acta* **26**, 1029 (1962).
- \_\_\_\_\_, *J. Geophys. Res.* **69**, 1995 (1964).
- R. O. Fournier and J. J. Rowe, *Am. J. Sci.* **264**, 685 (1966).
- W. G. Nelson and Tj. H. van Andel, *Mar. Geol.* **4**, 165 (1966).
- S. E. Humphris and G. Thompson, *Geochim. Cosmochim. Acta* **42**, 107 (1978).
- Manganese analyses were performed by G. Klinkhammer and M. Bender, University of Rhode Island.
- W. C. Shanks III and J. L. Bischoff, *Geochim. Cosmochim. Acta* **41**, 1507 (1977).
- M. R. Scott, R. B. Scott, P. A. Rona, L. W. Butler, A. J. Nalwalk, *Geophys. Res. Lett.* **1**, 355 (1974).
- W. S. Moore and P. R. Vogt, *Earth Planet. Sci. Lett.* **29**, 349 (1976).
- W. J. Jenkins, J. M. Edmond, J. B. Corliss, *Nature (London)* **272**, 156 (1978).
- H. Craig, W. B. Clarke, M. A. Beg, *Earth Planet. Sci. Lett.* **26**, 125 (1975).
- J. B. Corliss, J. M. Edmond, L. I. Gordon, *Proceedings of the Second Annual EWING Symposium* (American Geophysical Union, Washington, D.C., in press).
- R. N. Anderson, M. G. Langseth, J. G. Sclater, *J. Geophys. Res.* **82**, 3391 (1977).
- P. Lonsdale, *Deep-Sea Res.* **24**, 857 (1977).
- The clams were classified by K. Boss, Harvard University; the mussels by V. Kenk, San José State University; the limpets by J. McLean, Los Angeles County Museum of Natural History; the pogonophorans by M. Jones, National Museum of Natural History; and the fish photographs were examined by D. Cohen, National Museum of Natural History.
- The analyses of  $^{208}\text{Pb}$  were made by K. Turekian, Yale University.
- Microbiological studies were conducted by J. Baross, Oregon State University.
- C. R. B. Lister, *Tectonophysics* **41**, 157 (1977).
- B. Parsons and J. G. Sclater, *J. Geophys. Res.* **82**, 803 (1977).
- R. N. Anderson and M. A. Hobart, *ibid.* **81**, 2968 (1976).
- Deep Sea Drilling Project, Leg 54, *Geotimes* **22**, 19 (1977).
- E. A. Lubimova, R. P. Von Herzen, G. B. Udintsev, in *Terrestrial Heat Flow*, W. H. K. Lee, Ed. (American Geophysical Union, Monograph No. 8, Washington, D.C., 1965), p. 78.
- T. J. Chow and E. D. Goldberg, *J. Mar. Res.* **20**, 163 (1962).

64. R. M. Garrels and F. T. MacKenzie, *Evolution of Sedimentary Rocks* (Norton, New York, 1971).
65. L. H. Chan, J. M. Edmond, R. F. Stallard, W. S. Broecker, Y. C. Chung, R. F. Weiss, T. L. Ku, *Earth Planet. Sci. Lett.* **32**, 258 (1976).
66. F. R. Sclater, E. Boyle, J. M. Edmond, *ibid.* **31**, 119 (1976).
67. M. L. Bender, G. T. Klinkhammer, D. W. Spencer, *Deep-Sea Res.* **24**, 799 (1977).
68. The success of the expedition was made possible by the outstanding effort of the *Alvin* crew, under the direction of Larry Shumaker and Skip Marquet, the officers and crew of the R/V *Lulu*, Richard Flegenheimer, Master, and the R/V *Knorr*, Emerson Hiller, Master, and the members of the scientific party who carried out our heavy work schedule. Preliminary results from *Pleiades* leg 1 provided by P. Lonsdale, R. Weiss, J. Lupton and H. Craig are gratefully acknowledged. The expedition was funded by the Sea Bed Assessment program of the International Decade of Ocean Exploration Office, National Science Foundation; grant OCE 75-23352 to Oregon State University, and OCE 76-389 to Woods Hole Oceanographic Institution.

## Mobilizing Technology for Developing Countries

Charles Weiss, Jr.

The 15 years since the United Nations Conference on Science, Technology, and Development in Geneva have taught us that what seemed at first to be technological obstacles to development frequently turn out on closer examination to have been policy failures.

If economic policies prevent com-

continue to face severely restricted technological options.

If governments do not give high priority to the provision of safe water to poor people at a cost the country can afford, the agency charged with this responsibility will neither attract good managers, provide proper working conditions for its

**Summary.** A new problem in technology policy—a discipline hitherto largely concerned with the modern industrial sector—is posed by the need for technology suited to creating productive jobs and providing minimum public services at a cost and level of sophistication within the reach of poor people in developing countries. Careful consideration must be given to overall and sectoral development objectives, economic and manpower resources, and the local institutional and sociocultural context. This may indicate the need for both hardware innovation, such as low-cost alternatives to waterborne sewerage, and social (“software”) innovation, such as training large numbers of supervisors to implement improved technologies for labor-intensive civil works.

petition, firms will pass up opportunities for the use of known technology to improve quality. If financial authorities overvalue local currency, firms will have an incentive to import equipment and raw materials in place of locally available supplies and will neglect local sources of technology. If government marketing boards pay too little for higher quality, processors of agricultural commodities will neglect their machines and will fail to take advantage of improved technology. If banks are unwilling to extend credit to small farmers, the latter will

engineering staff, nor adopt appropriate design criteria, and hence will fail to employ the most suitable technology (1).

In each of these situations, the fact that a technology that seems suited to a local situation is, in fact, not used is a symptom of a deeper problem. In the language of experimental science, technology is a probe that reveals issues that might otherwise have escaped attention. But this does not mean that the problems thus revealed can necessarily be alleviated by the introduction of the “missing” technique. On the contrary, evidence is piling up that the impact of the introduction of any particular piece of equipment—whether tractors in south-

ern Asia (2) or waterless toilets in Vietnam (3)—depends heavily on the social and institutional structures on which it is superimposed.

For this reason, there are many situations in which an intervention focused purely on technology—whether indigenous or foreign and whether new, adapted, or transferred—is likely to be doomed from the start. In such cases, the introduction of hardware must be accompanied by and integrated with a package of policy and institutional changes if a desired innovation is to be effected, so it is more illuminating to refer to the institutional change necessary to the solution of a social problem as the “software” of the technology.

An example may make this point clearer. One may imagine three approaches to the problem of providing water to small farmers from aquifers near the surface: (i) designing and testing a small hand- or pedal-powered pump to be used by one or two farmers and encouraging a system to market and maintain such pumps; (ii) encouraging the installation of diesel-powered tube wells serving 50 or so farmers and ensuring an equitable distribution of the water through cooperatives; and (iii) encouraging entrepreneurs to hire out truck-mounted pumping equipment by the hour to individual farmers.

Each of these overall approaches—hardware plus institutional support—constitutes an alternative technology. The choice among them should depend on careful overall assessment of local technoeconomic, geographic, ecological, and social factors, as well as the desired balance between growth and equity. Such a technology assessment, a key element in the choice of “appropriate” (locally suitable) technology for particular investment projects, should be built into procedures for project preparation and appraisal in governments and development assistance agencies (4).

The crux of this approach is the focus on the problem rather than on the technology. “Technology is the answer—but what is the question?” (5). In the previous paragraphs, the objective is delivery of water, not development of pumps.

The author is Science and Technology Adviser at the World Bank, Washington, D.C. 20433.